Microporous Poly(tri(4-ethynylphenyl)amine) Networks: Synthesis, Properties, and Atomistic Simulation

Jia-Xing Jiang, Abbie Trewin, Fabing Su, Colin D. Wood, Hongjun Niu, James T. A. Jones, Yaroslav Z. Khimyak, and Andrew I. Cooper*

Department of Chemistry and Centre for Materials Discovery, University of Liverpool, Crown Street, Liverpool L69 7ZD, U.K.

Received November 22, 2008; Revised Manuscript Received February 24, 2009

ABSTRACT: Microporous poly(tri(4-ethynylphenyl)amine) networks were synthesized by palladium-catalyzed Sonogashira−Hagihara cross-coupling chemistry with apparent Brunauer−Emmet−Teller (BET) specific surface areas in the range 500−1100 m^2/g. It was found that very fine synthetic control over physical properties such as BET surface area, Langmuir surface area, micropore surface area, micropore volume, and bulk density could be achieved by varying the average monomer strut length. The micropore structure and micropore surface area were rationalized by atomistic simulations for one network, NCMP-0, based on multiple physical characterization data.

Introduction

There has been much interest recently in the synthesis of microporous materials such as metal−organic frameworks (MOFs),[1−5] covalent organic frameworks (COFs),[6−13] and organic polymers.[14−24] A recent development is the synthesis of conjugated microporous polymers (CMPs);[25] that is, highly conjugated organic materials with pore sizes of less than 2 nm. In our first two reports[25,26] we demonstrated the synthesis of conjugated microporous poly(aryleneethynylene) (PAE) networks with apparent Brunauer−Emmet−Teller surface area (S_{BET}) in the range 512−1018 m^2/g by Pd(0)/Cu(I)-catalyzed Sonogashira−Hagihara cross-coupling chemistry.[27] We also showed that the micropore size distribution and S_{BET} can be controlled by varying the length of the organic linker in the networks,[25,26] something which was previously thought to be the preserve of ordered crystalline materials such as MOFs[1−5] and COFs.[6−13] A number of other examples of CMPs (or closely related structures) have also appeared recently. For example, we reported alkyne−alkyne homocoupling as a route to conjugated microporous/mesoporous poly(phenylene butadiynylene)s (HCMPs)[28] (S_{BET} = 840 m^2/g). We also demonstrated the synthesis of a mesoporous poly(phenylenevinylene) (PPV) network with S_{BET} of 761 m^2/g.[29] Weber and Thomas have described both microporous poly(*p*-phenylene) and poly(phenyleneethynylene) materials based on a spirobifluorene building block (S_{BET} = 450−510 m^2/g).[30] Kaskel and co-workers[31] synthesized microporous hydrophobic polysilanes (S_{BET} up to 1046 m^2/g) via an organolithiation route. Kobayashi and co-workers[32,33] have also described recently the indirect preparation of porous pyrolytic polymers via treatment of alkyl-substituted poly(phenylenevinylene) precursors at high temperatures (>350 °C).

High surface area microporous materials are of general interest for applications such as gas storage, gas separations, and catalysis.[1−24] CMPs may also be interesting for other specific applications as a result of their conjugated structures. The physical properties of conjugated organic materials (e.g., conducting polymers, electroluminescent polymers, polymer photovoltaics) are frequently defined by the nature of physical interfaces.[34,35] This has been exploited, for example, in interpenetrating networks of electron donor and acceptor materials[36] and in hybrid polymer−metal oxide films for photovoltaic applications.[37] Highly microporous conjugated polymers are essentially "all interface" and can be conceptualized as interpenetrating networks where one of the interpenetrating components is free volume. This presents a number of opportunities: for example, the formation of composite materials with specific electronic or optoelectronic properties by in-filling of the micropore structure. The successful development of such strategies will require fine synthetic control over the pore structure of the CMP network. For example, it will be necessary to fine-tune physical properties such as physical surface area, pore volume (and bulk density, which is inversely related), average pore diameter, and pore connectivity and percolation. In some cases (e.g., hybrid polymer−metal oxide photovoltaics[37]) it may also be necessary to introduce donor or acceptor groups into the CMP network.

Organic polymer semiconductors derived from triphenylamine (TPA) derivatives have been widely investigated as hole-transporting or electroluminescent materials in organic light-emitting devices (OLEDs),[38−40] nonlinear optical materials,[41,42] and donor materials for solar cells.[43,44] In particular, Shirota and co-workers have developed a series of strategies to produce many classes of TPA-based compounds and polymers[38,39] but there are no reports concerning microporosity in this class of polymers.

We describe here a series of nitrogen-containing microporous polymers (NCMP) based on poly(triethynylphenyl)amine synthesized by Pd-catalyzed Sonogashira−Hagihara cross-coupling chemistry. Microporous NCMP networks were obtained with the highest apparent BET surface areas (up to 1108 m^2/g) yet reported for materials of this type. The average micropore size and S_{BET} was controlled by the molecular dimensions of the monomers employed, as found for CMP networks.[25,26] The porosity in network NCMP-0 was rationalized by atomistic molecular simulations and the "predicted" surface area agreed well with the micropore area. We also show that a range of physical properties (S_{BET}; Langmuir surface area; micropore surface area; micropore volume; bulk density) can be closely correlated with monomer strut length for both the CMP and NCMP networks series, much as observed for isoreticular MOFs.[4] This suggests broad potential for devising routes to new composite materials with fine control over the physical properties of the CMP or NCMP host network.

Experimental Section

Chemicals. 1,3,5-Triethynylbenzene was purchased from ABCR, tris(4-iodophenyl)amine was purchased from TCI, 1,4-diiodoben-

10.1021/ma802625d CCC: $40.75
Published on Web 03/16/2009

Table 1. Pore Structure Properties of NCMP-0−4

polymer	Alkyne monomer	Halogen monomer	S_{BET} $[m^2/g]$[a]	S_{MICRO} $[m^2/g]$[b]	V_{TOTAL} $[cm^3/g]$[c]	V_{MICRO} $[cm^3/g]$[d]
NCMP-0	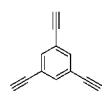	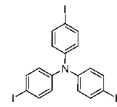	1108	825	0.60	0.51
NCMP-1	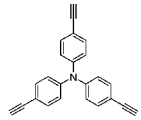	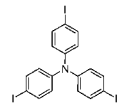	968	648	0.56	0.41
NCMP-2	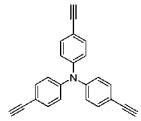	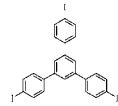	900	586	0.55	0.32
NCMP-3	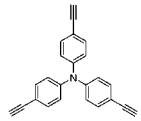		866	559	0.50	0.31
NCMP-4	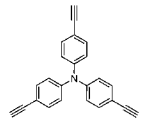	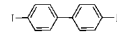	546	327	0.35	0.20

[a] Surface area calculated from the N_2 adsorption isotherm using the BET method. [b] Micropore surface area calculated from the N_2 adsorption isotherm using the *t*-plot method. [c] Total pore volume at $P/P_0 = 0.99$. [d] The micropore volume derived using the *t*-plot method based on the Halsey thickness equation.

zene, 4,4′-diiodobiphenyl, 1,3,5-tris(4-iodophenyl)benzene, tris(4-bromophenyl)amine, trimethylsilylacetylene, dichlorobis(triphenylphosphine)palladium(II), tetrakis(triphenylphosphine)palladium(0), copper(I) iodide, and other solvents were purchased from Aldrich and either recrystallized or used as received.

Synthesis of Tris(4-ethynylphenyl)amine. To a solution of tris(4-bromophenyl)amine (4.82 g, 10.0 mmol), copper(I) iodide (57 mg, 0.3 mmol) and dichlorobis(triphenylphosphine)palladium(II) (210 mg, 0.3 mmol) in diethylamine (40 mL) was added trimethylsilylacetylene (2.95 g, 30.0 mmol) dropwise under a nitrogen atmosphere. The mixture was heated to 50 °C and stirred for 12 h. After cooling to room temperature, the precipitate that was formed was filtered and washed with ether. The combined filtrates were evaporated under reduced pressure and the crude product was purified by column chromatography (Silica Gel, light petroleum) to give tris-(4-trimethylsilylethynyl)phenylamine as an intermediate. Hydrolysis of this compound was carried out by treatment with a mixture of MeOH (50 mL)/NaOH (50 mL, 1 M) with stirring at room temperature for 12 h. Standard workup involved evaporation of the organic solvent, extration of the residue with ether, drying with Mg_2SO_4 overnight, and removal of the solvent under reduced pressure. The crude product was purified by column chromatography (silica gel, light petroleum) to give tris(4-ethynylphenyl)amine as a white solid (2.5 g, Yield: 78.8%). ^{1}H NMR ($CDCl_3$), δ (ppm): 7.35 (d, 6H), 6.47 (d, 6H), 3.15 (s, 3H). ^{13}C NMR ($CDCl_3$), δ (ppm): 140.75, 133.26, 123.45, 118.24, 83.47. 78.26. Anal. Calcd for $C_{24}H_{15}N$: C, 90.85; H, 4.73; N, 4.42. Found: C, 90.47; H, 4.69; N, 4.38. Mass *m*/*z*: 335.24 $[M + NH_4]^+$.

Synthesis of Poly(triethynylphenyl)amine Networks. All of the poly[tris(ethynylphenyl)amine] networks were synthesized by palladium-catalyzed Sonogashira−Hagihara cross-coupling condensation reaction of aryl ethynylenes and aryhalides.[27] A representative experimental procedure for NCMP-0 is given below:[45]

NCMP-0. 1,3,5-Triethynylbenzene (450.5 mg, 3 mmol), tris(4-iodophenyl)amine (1246 mg, 2.0 mmol), tetrakis(triphenylphosphine)palladium(0) (35 mg, 0.03 mmol), and copper(I) iodide (7 mg, 0.03 mmol) were dissolved in the mixture of toluene (4 mL) and Et_3N (4 mL). The reaction mixture was heated to 80 °C and stirred for 72 h under a nitrogen atmosphere (in order to rigorously exclude oxygen and to prevent any homocoupling of the alkyne monomers). The mixture was cooled to room temperature and the insoluble precipitated network polymer was filtered and washed four times with chloroform, water, methanol, and acetone to remove any unreacted monomers or catalyst residues. Further purification of the polymer was carried out by Soxhlet extraction with methanol for 48 h. The product was dried in vacuum for 24 h at 70 °C and isolated as a fine light brown powder (Yield: 73.4%). FTIR (KBr cm^{-1}): 3300.7 (−C≡C−H), 2206.8 (−C≡C−). Anal. Calcd for $C_{30}H_{15}N$: C, 92.54; H, 3.86; N, 3.60. Found: C, 86.55; H, 4.08; N, 2.89; I, 1.21. The deviation of the elemental analysis from theory can be accounted for by the unreacted alkyne-, and iodo-phenyl end groups indentified by solid-state NMR as well as (to a lesser degree) catalyst residues identified by EDX.

All polymerization reactions were carried out at a fixed total molar monomer concentration (625 mmol/L) and a fixed reaction temperature and reaction time (80 °C/72 h). The molar ratio of ethynyl to halogen functionalities in the monomer feed was set at 1.5:1 based on our previous findings for CMP networks.[25,26]

Gas Sorption: Surface Areas, Pore Size Distributions, and H_2 Uptakes. Polymer surface areas and pore size distributions were measured by nitrogen adsorption and desorption at 77.3 K using either a Micromeritics ASAP 2420 or ASAP 2020 volumetric adsorption analyzer. The surface areas were calculated in the relative pressure (P/P_o) range from 0.05 to 0.20. Pore size distributions and pore volumes were derived from the adsorption branches of the isotherms using the nonlocal density functional theory (NL-DFT). Samples were degassed at 110 °C for 15 h under vacuum (10^{-5} bar) before analysis. Hydrogen isotherms were measured at 77.3 K up to 1.13 bar using a Micromeritics ASAP 2420 volumetric adsorption analyzer.

Solid-State NMR. Solid-state NMR spectra were measured on a Bruker Avance 400 DSX spectrometer operating at 100.61 MHz

for ^{13}C and 400.13 MHz for ^{1}H. $^{1}H-^{13}C$ cross polarization magic angle spinning (CP/MAS) NMR experiments were carried out at a MAS rate of 10.0 kHz using zirconia rotors of 4 mm in diameter. The ^{1}H $\pi/2$ pulse was 3.1 μs and two pulse phase modulation (TPPM) decoupling[46] was used during the acquisition. The Hartmann−Hahn condition was set using hexamethylbenzene. The spectra were measured using contact time of 2.0 ms and relaxation delay of 8.0 s. Typically 2048 scans were accumulated. The variable contact time $^{1}H-^{13}C$ CP/MAS NMR spectra were measured using t_m= 0.01−16.0 ms. The $^{13}C/^{1}H$ MAS NMR spectra were measured at MAS rate of 10.0 kHz using TPPM decoupling. The ^{13}C $\pi/3$ pulse was 2.6 μs. The spectra were measured using the recycle delay of 30.0 s. Typically 1024 scans were accumulated. The values of chemical shift are referred to TMS. The analysis of the spectra (deconvolution and integration) was carried out using Bruker TOPSPIN software.

Atomistic Simulations. Molecular models for the NCMP-0 networks were generated using the *Materials Studio Modeling 4.0* package (Accelrys Inc., San Diego, CA, 2005).

(i) Fragment Models, NCMP-0−NMCP-4. Small fragments of all five NCMP networks were constructed by combining the relevant tris(alkynyl) monomer with the corresponding halogenated monomer (see Table 1) in a stepwise manner to yield fragments each with 28 N-containing monomer subunits.

(ii) Amorphous Cell Simulation, NCMP-0. A larger model was also constructed for NCMP-0 in order to simulate the micropore structure in this material. Again, the monomers (1,3,5-triethynylbenzene and 1,3,5-tris(4-iodophenyl)benzene in this case) were combined in a stepwise manner. Two slightly different cluster models were constructed: one which imposed significant $\pi-\pi$ stacking between adjacent monomers (total cluster molecular weight = 24,474 g/mol) and another more amorphous model (molecular weight = 26,108 g/mol). In the first model, the $\pi-\pi$ stacking was introduced by manually constructing small planar π-stacked subunits which were then connected to form the larger cluster. By contrast, in the more amorphous model whole cluster was constructed in a single step and then four such clusters were combined in the amorphous cell before minimization. The result was two models, one in which $\pi-\pi$ stacking is very dominant and a second amorphous model where $\pi-\pi$ stacking also occurs naturally after minimization but to a lesser degree. Each cluster model was built to have the same number of the 1,3,5-tris(iodophenyl)amine repeat units. The amorphous cell module in Materials Studio 4.0 was used to construct a three-dimensional amorphous simulation cell for each of these models which contained four of the respective clusters. The target bulk density for the simulation was set to 0.83 g/cm^3 as calculated from the experimental micropore volume (0.51 cm^3/g) and the absolute density as measured by helium pycnometry (1.4567 g/cm^3).[21] The models were further refined by fitting with additional physical characterization data. First, NMR data suggested that the material contained approximately 10 wt % terminal alkyne end groups. Second, elemental analysis showed the composition to be as follows: C, 86.48; H, 4.05; N, 2.90; I, 1.21. Thus, three further targets were set for the atomistic simulations: (i) unreacted iodophenyl end groups were included to achieve an overall 1.2 wt % iodine loading in the simulation; (ii) the number of 1,3,5-tris(iodophenyl)amine repeat units per cell was set to achieve ∼2.90 wt % N; (iii) the number of terminal alkyne end groups per unit cell was set to achieve 10 wt % in the simulation. Any remaining iodophenyl/ethynylbenzene end groups were manually connected by removing the surplus iodine and hydrogen. In this way it was possible to construct a simulation cell with overall properties which agreed very closely with all of the available physical characterization data for NCMP-0 (i.e., bulk density, absolute density, pore volume, elemental composition). All models were fully relaxed using the *Discover* molecular mechanics and dynamics simulation module with the COMPASS forcefield.[21,47] Surface areas were estimated from these simulations from the solvent accessible surface (probe radius = 1.82 Å) using the methodology set out by Düren et al.[48] The Connolly surface area is calculated by rolling a probe molecule across the substrate, the interface taken from the contact point of the probe molecule. For the accessible surface, the surface area is calculated from the center of the probe molecule. We calculated the solvent-accessible surface area which is equivalent to the accessible surface area,[48] but only takes into account free volume which can be accessed from at least one of the six sides of the amorphous cell simulation box.

Results and Discussion

Synthesis and Properties of Networks NCMP-0−NCMP-4. The monomers used to prepare a series of five NCMP networks and the resulting physical properties of these networks are summarized in Table 1. The networks were designed to have a three-dimensional net structure arising from the three-pronged aryl linkages (Scheme 1). Thermal analysis for the networks showed no evidence for any glass transition or melting point below the thermal decomposition temperature for the materials (>300 °C in all cases under N_2). All of the networks were chemically stable, for example, to dilute solutions of acids and bases such as HCl and NaOH. Moreover, the relatively harsh work up conditions (>48 h Soxhlet extraction, MeOH) did not significantly reduce porosity or surface area with respect to materials purified by simple washing; again, this is consistent with good physicochemical robustness for these NCMP networks.

All polymers were characterized by $^{1}H-^{13}C$ CP/MAS NMR. The assignment of the resonances for these NCMP networks was more complex than for our previous microporous CMP materials,[25,26] which did not contain any nitrogen atoms. However, resonances due to tris(phenylethynylene)amine units and aryleneethynylene units which do not bear the nitrogen atoms were easily distinguished. The assignment of the resonances (Figure 1) is consistent with spectra reported previously for CMP networks[25,26] and was confirmed by $^{13}C/^{1}H$ MAS NMR spectra and $^{1}H-^{13}C$ CP/MAS NMR kinetics. Ethynylene $C_{ar}-\mathbf{C}\equiv\mathbf{C}-C_{ar}$ units are observed at *ca.* 90 ppm and show the slowest CP-kinetics. The low intensity resonances at ca. 76 and 82 ppm can be ascribed to the −C≡CH end groups with the line at ca. 82 ppm corresponding to the quaternary acetylenic end group. The content of these end groups was highest for network NCMP-0, but does not exceed ca. 15% even for this network. The quaternary $N-\mathbf{C}_{ar}$ sites exhibit a peak at *ca.* 147 ppm. The $\mathbf{C}_{ar}-C\equiv C$ sites for tris(phenylethynylene)amine units are observed at *ca.* 120 ppm. These sites are observed for all five of the NCMP networks. The $-\mathbf{C}_{ar}-\mathbf{C}_{ar}-$ linkages in NCMP-2 and NCMP-4 are observed at *ca.* 141 ppm. The lines at *ca.* 127 ppm in these networks originate from the $H-C_{ar}-$ sites in the aromatic rings *not* connected with nitrogen. The $-C\equiv C-\mathbf{C}_{ar}$ sites in such benzene rings are observed at *ca.* 124 ppm. The ratio of the intensities of the acetylenic and aromatic peaks was calculated using the $^{13}C/^{1}H$ MAS NMR spectra as follows: NCMP-0, 0.23 (expected value 0.25); NCMP-1, 0.11 (expected value 0.17); NCMP-2, 0.12 (expected value 0.14); NCMP-3, 0.18 (expected value 0.22); NCMP-4, 0.12 (expected value 0.17).

The porous structure of the NCMP networks was investigated by sorption analysis using N_2 and H_2 as the sorbate molecule. Figure 2a shows the N_2 adsorption and desorption isotherms for the resulting polymers. All NCMP networks gave rise to type I N_2 gas sorption isotherms[49] indicating that the networks are microporous. Somewhat more hysteresis was observed upon desorption than was apparent for analogous PAE networks.[25,26] The apparent BET surface area for these networks varied between 546 m^2/g (NCMP-4) and 1108 m^2/g (NCMP-0) (Table 1). The BET surface area for NCMP-0 is higher than observed for any of a range of analogous networks reported recently[25,26,28−31] and in excess of the highest S_{BET} reported thus far for polymer of intrinsic microporosity (PIM).[17] Figure 2b shows pore size distribution curves for the five NCMP networks

Scheme 1. Representative Molecular Structures for Networks NCMP-0−4[a]

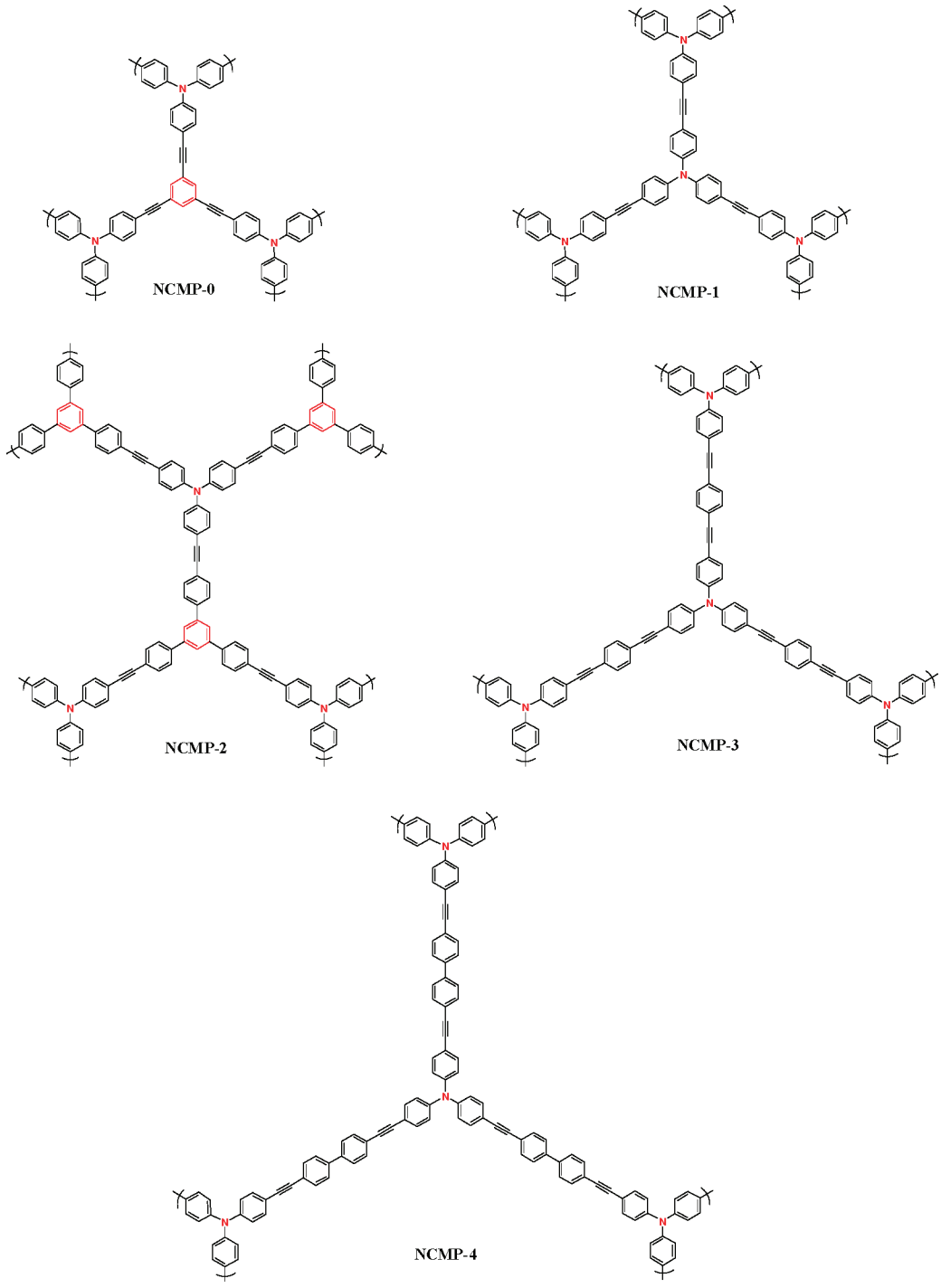

[a] The nitrogen and benzene "nodes" in the networks (derived from the trifunctional A_3 or B_3 monomer in each case) are shown in red.

as calculated using nonlocal density functional theory (NL-DFT). NL-DFT does not take into account swelling effects which may be important in the case of polymer networks. Indeed, there is no perfect model for describing micropore size distributions in these materials, however NL-DFT has been applied previously to polymers[24,25] and to COFs[6,9] and shown (in the case of COFs) to give pores sizes which correlate broadly with structural X-ray diffraction data. Figure 2b and 2c show that the micropore size distribution is shifted systematically to larger pore diameters for the series NCMP-0 to NCMP-4 and the overall micropore volume falls concomitantly from 0.51 to 0.20 cm^3/g. This is also illustrated by NL-DFT cumulative pore volume plots for the five networks (Figure 2c). These observations are consistent with our previous results[25,26] and further illustrate that micropore dimensions and surface area can be tuned synthetically by varying the monomer strut length in amorphous PAE networks.

The hydrogen sorption properties of the polymers were also investigated by volumetric methods (see Supporting Information).[19,21] As would be expected, NCMP-0 which has the highest micropore volume and highest S_{BET}, exhibited the largest H_2 uptake of 165 cm^3/g at 1.13 bar/77.3 K (~1.5 wt %; ~2.0 wt % at 8 bar, see Supporting Information, Figures S3 and S4). The H_2 tracked S_{BET} and the micropore volume, V_{MICRO}, for NCMP-0−4 (Figure S3).

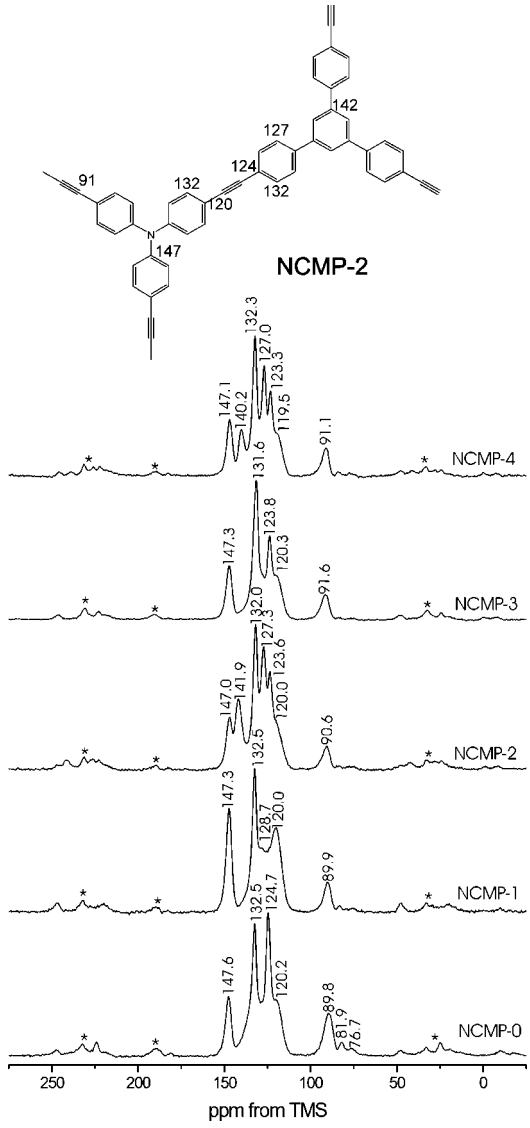

Figure 1. Solid-state $^{1}H-^{13}C$ CP/MAS NMR spectra of networks NCMP-0−4 recorded at MAS rate of 10 kHz. Asterisks denote spinning sidebands. The subunit structure for NCMP-2 contains all of the possible carbon environments and hence has a more complex NMR spectrum; this is shown as a guide to the assignment of the various resonances.

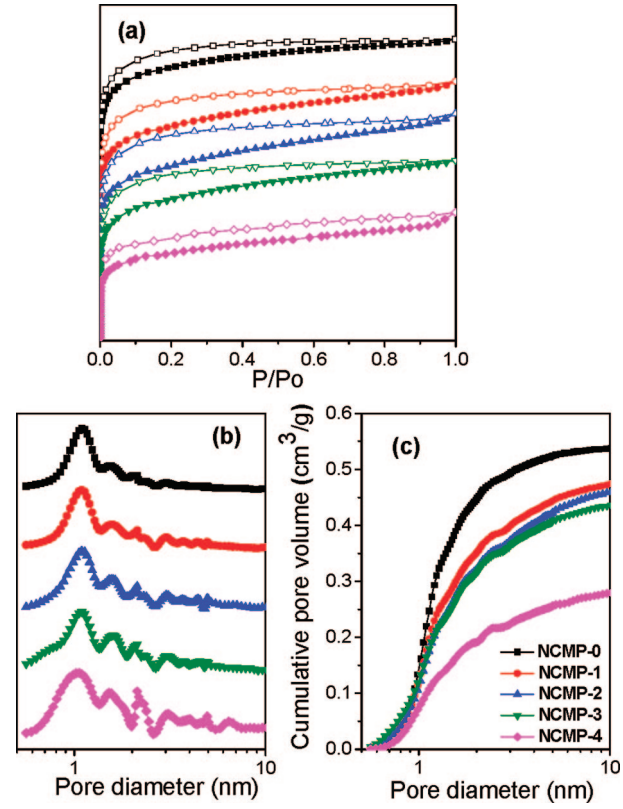

Figure 2. (a) N_2 adsorption−desorption isotherms measured at 77.3 K (adsorption branch is labeled with filled symbols, data are vertically offset in for clarity). (b) NL-DFT pore size distribution curves. (c) Cumulative pore volume curves calculated by application of NL-DFT.

While the porosity varies quite smoothly in this series of materials, some other properties are more discontinuous. For example, as a result of its structure, NCMP-1 has around double the nitrogen content (4.36 wt % versus ~2 wt %; see Supporting Information) of the other four networks.

Our previous studies have rationalized the trend in S_{BET} for a series of conjugated microporous PAE homopolymers, CMP-0 to CMP-5,[25,26] as well statistical copolymers, CPN-1 to CPN-6,[26] on the basis of the average simulated monomer "strut length", L_{AV}. Molecular simulations for small subclusters of these NCMP materials suggested that the amorphous nature of these kinetically formed networks arises from facile rotation around the aryleneethynylene bond (primary influence) as well as bending of monomer struts out of plane of the benzene nodes, bending of the struts themselves, and from in-plane deviation of the angle between struts from the hypothetical 120° imposed by the 1,3,5-substituted geometry. Figure 3 shows a series of simulated fragment clusters for networks NCMP-0 to NCMP-4 showing the effect of increasing average "strut" length. The average strut length, L_{AV}(strut), calculated from simulations for this range of materials (as well as the series CMP-0 through CMP5[25,26] and CPN-2 through CPN-5[26]) are tabulated in order of increasing magnitude in the Supporting Information (Table S1). Both L_{AV}(strut) and the average overall cluster diameter, L_{AV}(cluster), increase in the series NCMP-0 to NCMP-4. We believe that the increased degree of conformational freedom in the longer struts allows for greater intermolecular and intramolecular intercalation and more efficient space filling in the structures, and that this contributes to the decreased micropore volume for networks with longer struts. NCMP-4 does not have the largest pore volume: indeed, the reverse is true and NCMP-4 has the highest density and lowest pore volume in this series. By contrast, networks with shorter struts possess a greater number of small-diameter pores (and hence higher surface areas) due to the rigidity and relative lack of conformational freedom for these struts.

Figure 4 shows a "global" physical properties plot for a series of 14 different PAE networks: CMP0−CMP5,[25,26] CPN2−CPN5,[26] and this new series of NCMP networks, NMCP-0-NMCP-4. Five different physical properties are represented, all of which would be important in terms of designing, for example, possible interpenetrating electroactive composite materials. These five properties are; (i) the BET surface area, S_{BET}, as calculated from the N_2 isotherm; (ii) the Langmuir surface area, S_{LANG}, as calculated from the H_2 isotherm; (iii) micropore surface area, S_{MICRO}; (iv) the micropore volume, V_{MICRO}; (v) the bulk density, ρ. The materials are placed in order of calculated average strut length (L_{AV}) from atomistic simulations. As can be seen, the CMP/CPN series[25,26] and NCMP series are interspersed when ordered in this way. There is a systematic increase in V_{MICRO} and in all three measures of surface area (S_{BET}, S_{LANG}, S_{MICRO}) as L_{AV} is decreased. Similarly, the bulk density, ρ, decreases with decreasing L_{AV}. The very systematic variation of properties with L_{AV} is particularly noteworthy given

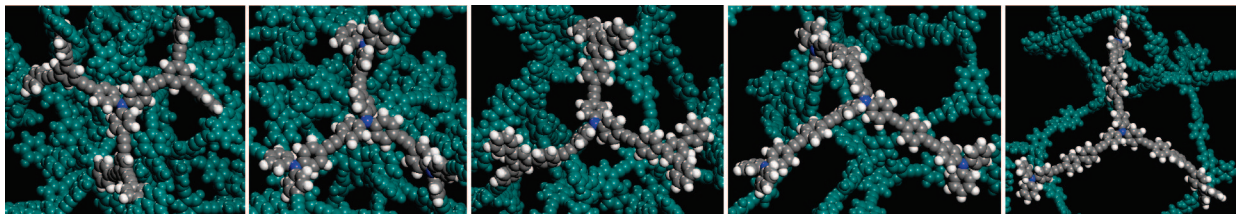

Figure 3. Atomistic simulations for fragments of NCMP networks with different strut lengths. Node-strut topology for simulated network fragments for, from left to right, NCMP-0, NCMP-1, NCMP-2, NCMP-3, and NCMP-4. A 1,3,5-tris-phenylamine node connecting to three other nodes via rigid struts is highlighted (in gray/white) in each case. Note that these are energy-minimized fragment models only. No attempt was made to pack or interpenetrate these fragments (see simulation discussion, below) and hence NCMP-4 does not have the largest pore volume: indeed, the reverse is true and NCMP-4 has the highest density and lowest pore volume in this series.

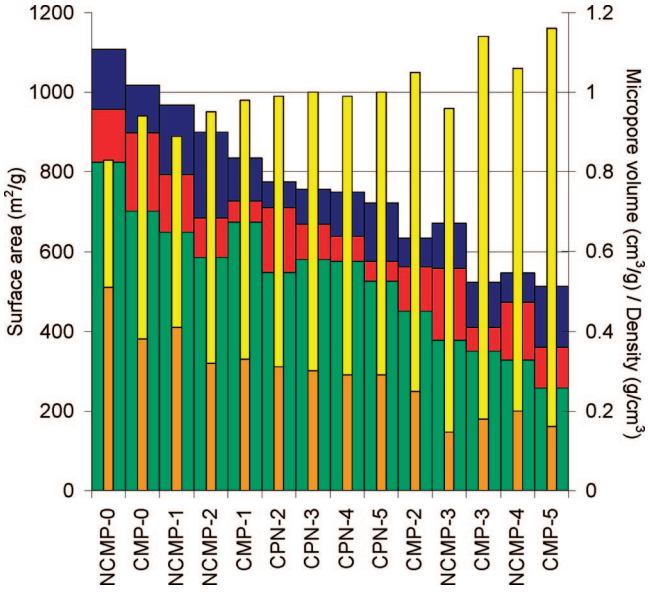

Figure 4. Plot showing the N_2 BET surface area (S_{BET}, dark blue), H_2 Langmuir surface area (S_{LANG}, red), N_2 micropore surface area (S_{MICRO}, green), N_2 micropore volume (V_{MICRO}, orange) and bulk density (ρ, yellow) for a range of NCMP, CMP, and CPN networks plotted in order of increasing calculated strut length, L_{AV}. All of these values (including L_{AV}) are also tabulated in the Supporting Information.

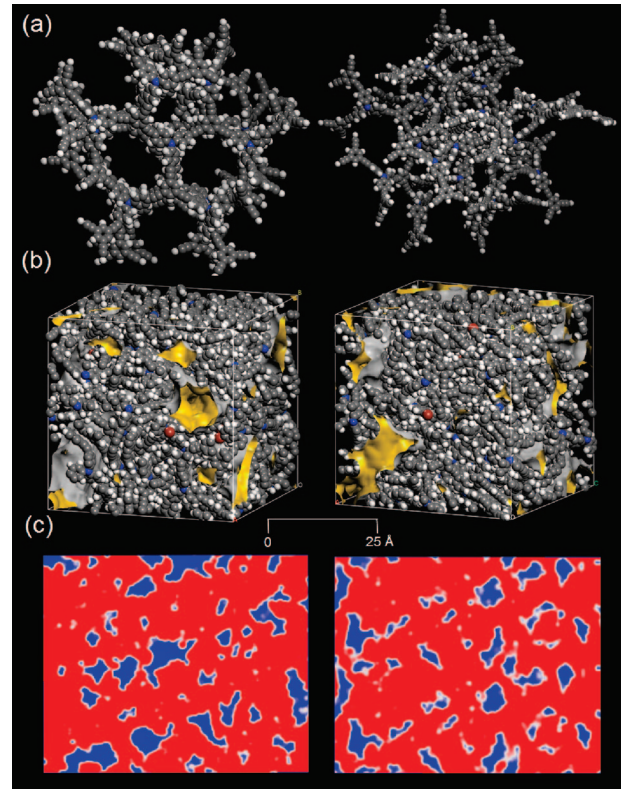

Figure 5. Atomistic simulations for the two proposed models for NCMP-0 (a) Clusters of NCMP-0 used to build the amorphous cells. Left: cluster containing significant $\pi-\pi$ stacking. Right: amorphous cluster. Both clusters were built to contain 28 N atoms (blue spheres). (b) Amorphous cells constructed from the $\pi-\pi$ stacked cluster (left) and amorphous cluster (right). A solvent accessible surface is also shown (yellow/gray) for both models. (c) Two-dimensional "slice" through an array of amorphous cells in the simulated pore structure. The occupied and unoccupied volumes are shown in red and blue respectively.

that the three series of materials (CMP,[25,26] CPN,[26] and NCMP) were synthesized in consecutive batches and not in a single "designed run". This level of direct synthetic fine-tuning of micropore properties is unprecedented for amorphous materials and rivals that achieved for a series of isoreticular MOFs with different strut lengths,[4] although the property ranges obtained are different (e.g., N_2 Langmuir SA for IRMOF-6 = 2630 m^2/g). There are other fundamental differences between our amorphous PAE materials and the crystalline IRMOF series.[4] First, the physical properties for these PAE networks scale simply with, and in almost precise order of, calculated average monomer strut length, L_{AV} (Figure 4). This is not the case for the IRMOF series where such ordering of properties is also affected by linker functionalization and the existence of concentration-dependent interpenetrating/noninterpenetrating structural counterparts (e.g., IRMOF-9/IRMOF-10).[4] Comparable "periodicity" of physical properties does not occur in these amorphous PAE networks since they can all be considered as interpenetrating but in a less binary and more statistical sense. This allows even finer tuning of properties via the preparation of statistical copolymers.[26] The second obvious difference is that the "strut length" trends are essentially reversed: longer alkyne struts lead to higher bulk densities (and lower S_{BET}, V_{MICRO}, etc., as rationalized above) whereas increasing the linker length in IRMOFs results generally in lower crystal densities and higher free volumes.[4] The range of micropore/mesopores volumes that can be accessed for IRMOFs is significantly broader than is possible in this PAE series. Direct synthetic fine-tuning of micropore properties in COFs has also been achieved by varying the alkyl groups that were incorporated within the pores.[13]

Atomistic Simulation of Micropore Properties, NCMP-0. In our previous studies involving microporous PAEs[25,26] we simulated small fragments of the networks (*cf.*, Figure 3) but these models are not representative of the actual pore structure for the materials. To do that, it is necessary to construct a model which simulates the bulk density of the real networks by allowing for packing and interpenetration of fragments.[21,24] An amorphous cell was therefore built for the NCMP-0 network to match the measured bulk density (0.83 g/cm^3)[50] and other characterization data for this material (see Experimental Section). It was noted

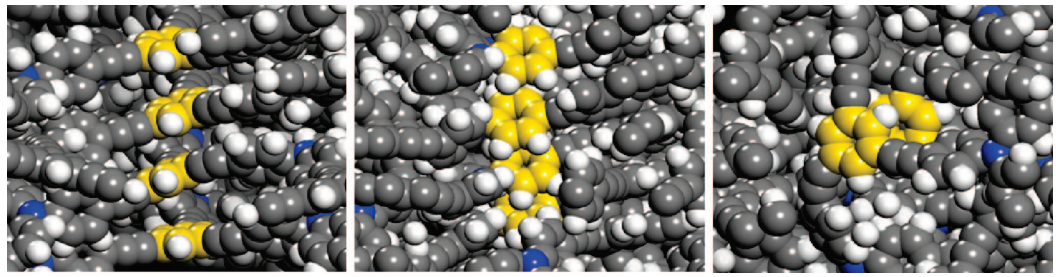

Figure 6. Atomistic simulations for the two proposed models for NCMP-0 highlighting areas exhibiting $\pi-\pi$ stacking (yellow). Left: $\pi-\pi$ stacked cluster before formation of amorphous cell. Center: the amorphous cell constructed using the $\pi-\pi$ stacked cluster, average distance between p-stacked benzene rings = 4.33 Å. Right: amorphous cell constructed using the amorphous cluster, average distance between p-stacked benzene rings = 4.11 Å.

Table 2. "Amorphous" and $\pi-\pi$ Stacked Models of NCMP-0

cluster model	Connolly surface area (m^2/g)[a]	solvent accessible surface area (m^2/g)[b]	energy (kJ mol^{-1} $Å^{-3}$)[c]	energy (kJ mol^{-1})[d]
"amorphous"	2524	750	−0.25	−241
$\pi-\pi$ stacked	2334	741	−0.27	−257

[a] Connolly Surface area and [b] Solvent accessible surface area, both calculated using a probe molecule with radius = 0.182 nm (kinetic radius of N_2). [c] Free energy of the simulated material calculated per cubic Å. [d] Free energy calculated per N node within the simulation box.

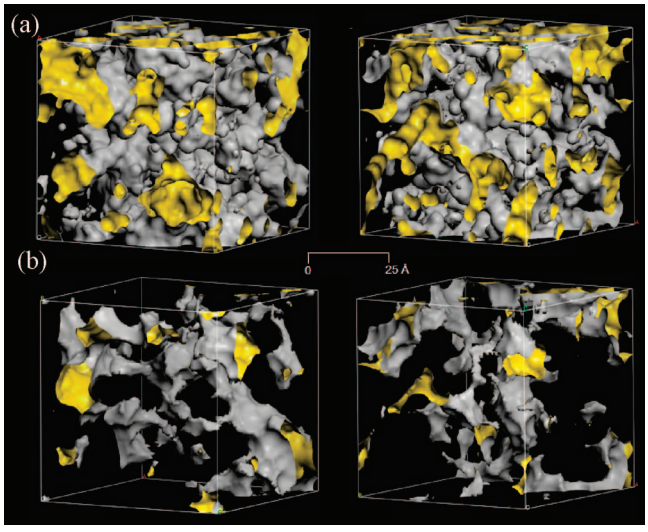

Figure 7. Simulated Connolly surfaces (a) and solvent accessible surfaces (b) (both shown in yellow/gray) for (left) π-stacked model and (right) amorphous model.

during the construction of the NCMP-0 cluster that areas of $\pi-\pi$ stacking between the 1,3,5-trisubstituted benzene nodes were formed spontaneously during energy minimization. To investigate this further, an alternative cluster containing "forced" $\pi-\pi$ stacks was also built (Figure 5a; see Experimental Section for full methodology). Both models led to simulations with pronounced $\pi-\pi$ stacking (Figure 6) although this was more prominent when stacking was "built into" the cluster prior to packing and minimization of the amorphous cell.[51]

It is difficult to compare absolute energies for these two simulations reliably; however, we did attempt to compare the relative energies of the models by two different metrics: (i) the energy per unit volume of the simulation cell; (ii) the energy N-node (there are equal numbers of nodes in each cell). Both of these methods suggested that the simulation cell containing more significant $\pi-\pi$ stacking was energetically favored. This is supported by numerous experimental studies which show evidence for favorable $\pi-\pi$ stacking in triphenylamine-derivatized polymers[52] and other conjugated materials,[35] although bulky alkoxy-functionalized triphenylamine groups have also been used to suppress $\pi-\pi$ stacking in some linear polymers.[53]

The Connolly surface area and solvent accessible surface area[48] were calculated for both the amorphous and the $\pi-\pi$ stacked models, Figure 5b,c. The values obtained for both models were very similar (Table 2). The simulated solvent accessible surface areas (750 and 741 m^2/g) were in fairly good agreement with the experimental micropore surface area (825 m^2/g) for both models, while the Connolly surface area (>2300 m^2/g) greatly overestimated the physical surface, as found previously for other systems.[24,48] It should be noted that these models represent micropore structure only: the amorphous simulation cell is of the order of 3 × 3 × 3 nm and, as such, these simulations will not account for any larger pores (e.g., mesopores >2 nm).[50] Although NCMP-0 is predominantly microporous (see Figure 2, Table 1), the cumulative NL-DFT pore size distribution curve (Figure 2c) does suggest a small percentage of mesoporosity which will not be accounted in these simulations(V_{MICRO} = 0.51 cm^3/g; V_{TOTAL} = 0.60 cm^3/g). As such, comparison of the simulated values with S_{MICRO} (rather than S_{BET} or S_{LANG}) is more appropriate since these models will fail to represent larger interconnected mesopores that are present in some degree in the real NCMP-0 material.

For many applications such as interpenetrating composites, pore connectivity and percolation will be important in addition to pore size and pore volume. This is challenging to probe directly and the simulation representations shown in Figure 5, parts b and c, do not give a good indication of this property for these bicontinuous structures. Figure 7 shows the simulated Connolly and solvent accessible surfaces in the absence of the atoms in the material. The accessible surface depends of course on the specific sorbate probe—in this case, we used the kinetic radius of nitrogen (1.82 Å) which was the sorbate gas used for most of the sorption characterization (Figure 2). The Connolly surfaces (Figure 7, left) greatly overestimate the level of pore connectivity in the networks with respect to real sorbates such as N_2. The solvent accessible surfaces, however, most likely give a more realistic picture, at least for the materials in the dry, unswollen state (Figure 7, right). Again, as discussed above, some porosity in the real materials (small mesopores) is not represented in these simulations and this most likely enhances pore connectivity. Even a simulation of the micropore structure only,[50] however, suggests that the pore structure may be moderately well interconnected at this bulk density. These simulations (and the micropore size distributions, Figure 2b) imply that it may be difficult to imbibe some molecules of interest (e.g., metal oxide precursors)[37] into parts of the micropore structure because they will be size excluded. This may however be facilitated by interconnecting small mesopores which are not simulated here but which are present in the real NCMP-0 material. Also, these are static simulations: in reality, swelling will occur upon contact with solvents, although

probably not with gaseous N_2 or H_2 under the (P,T) conditions studied here. Indeed, some hypercrosslinked polystyrenes swell enormously (>10-fold weight increases) in the presence of organic solvents and even significantly in "bad" solvents such as water.[19−21,54] Our studies suggest that these PAE networks are not as generally swellable as these hypercrosslinked polystyrene materials[19−21,54] but that they are capable of swelling to some degree and adsorbing significant quantities of common organic solvents.

Conclusion

A series of microporous poly[tris(ethynylphenyl)amine] networks was synthesized by using palladium-catalyzed Sonogashira−Hagihara chemistry. The polymers are chemically and thermally stable and are composed solely of carbon−carbon, carbon−nitrogen, and carbon−hydrogen bonds. There is a wealth of opportunity for producing porous materials with specific functionality: for example, by attaching metals to the network to facilitate catalysis or to introduce high-binding energy sites such as metals[55−57] "naked" halides,[58] or transition metal complexes[59] for H_2 storage. These findings also suggest the possibility for producing composite photovoltaic materials or conducting microporous materials facilitated by the ability to incorporate donor functionality such as triphenylamine moieties. For example, these NCMP materials or similar networks might be doped with molecules such as 7,7,8,8-tertracyno-*p*-quinodimethane (TCNQ) or iodine.[60] The postsynthetic modification of these networks with a variety of organic and inorganic functionalities is currently in progress, as is the introduction of tetrahedral linking monomers.[61]

Acknowledgment. The authors are grateful to EPSRC (EP/C511794/1 & EP/F057865/1) and the University of Liverpool for financial support.

Supporting Information Available: Text discussing the synthesis of NCMP-1 to NCMP-4, a table giving the physical properties of NCMP-0−4 compared with other CMP networks, and figures showing solid-state NMR data, and volumetric H_2 adsorption isotherms for NCMP-0−4. This material is available free of charge via the Internet at http://pubs.acs.org.

References and Notes

(1) Yaghi, O. M.; Li, H. L.; Davis, C.; Richardson, D.; Groy, T. L. *Acc. Chem. Res.* **1998**, *31*, 474–484.
(2) Cheetham, A. K.; Férey, G.; Loiseau, T. *Angew. Chem., Int. Ed.* **1999**, *38*, 3268–3292.
(3) Li, H.; Eddaoudi, M.; O'Keeffe, M.; Yaghi, O. M. *Nature* **1999**, *402*, 276–279.
(4) Eddaoudi, M.; Kim, J.; Rosi, N.; Vodak, D.; Wachter, J.; O'Keeffe, M.; Yaghi, O. M. *Science* **2002**, *295*, 469–472.
(5) Kitagawa, S.; Kitaura, R.; Noro, S. *Angew. Chem., Int. Ed.* **2004**, *43*, 2334–2375.
(6) Côté, A. P.; Benin, A. I.; Ockwig, N. W.; O'Keeffe, M.; Matzger, A. J.; Yaghi, O. M. *Science* **2005**, *310*, 1166–1170.
(7) Tilford, R. W.; Gemmill, W. R.; zur Loye, H. C.; Lavigne, J. J. *Chem. Mater.* **2006**, *18*, 5296–5301.
(8) Côté, A. P.; El-Kaderi, H. M.; Furukawa, H.; Hunt, J. R.; Yaghi, O. M. *J. Am. Chem. Soc.* **2007**, *129*, 12914–12915.
(9) El-Kaderi, H. M.; Hunt, J. R.; Mendoza-Cortes, J. L.; Côté, A. P.; Taylor, R. E.; O'Keeffe, M.; Yaghi, O. M. *Science* **2007**, *316*, 268–272.
(10) Mastalerz, M. *Angew. Chem., Int. Ed* **2008**, *47*, 445–447.
(11) Kuhn, P.; Antonietti, M.; Thomas, A. *Angew. Chem., Int. Ed* **2008**, *47*, 3450–3453.
(12) Han, S. S.; Furukawa, H.; Yaghi, O. M.; Goddard, W. A. *J. Am. Chem. Soc.* **2008**, *130*, 11580–11581.
(13) Tilford, R. W.; Mugavero, S. J.; Pellechia, P. J.; Lavigne, J. J. *Adv. Mater.* **2008**, *20*, 2741–2746.
(14) Budd, P. M.; Ghanem, B. S.; Makhseed, S.; McKeown, N. B.; Msayib, K. J.; Tattershall, C. E. *Chem. Commun.* **2004**, 230–231.
(15) McKeown, N. B.; Gahnem, B.; Msayib, K. J.; Budd, P. M.; Tattershall, C. E.; Mahmood, K.; Tan, S.; Book, D.; Langmi, H. W.; Walton, A. *Angew. Chem., Int. Ed.* **2006**, *45*, 1804–1807.
(16) Budd, P. M.; Butler, A.; Selbie, J.; Mahmood, K.; McKeown, N. B.; Ghanem, B.; Msayib, K.; Book, D.; Walton, A. *Phys. Chem. Chem. Phys.* **2007**, *9*, 1802–1808.
(17) Ghanem, B. S.; Msayib, K. J.; McKeown, N. B.; Harris, K. D. M.; Pan, Z.; Budd, P. M.; Butler, A.; Selbie, J.; Book, D.; Walton, A. *Chem. Commun.* **2007**, 67–69.
(18) Germain, J.; Hradil, J.; Fréchet, J. M. J.; Svec, F. *Chem. Mater.* **2006**, *18*, 4430–4435.
(19) Lee, J. Y.; Wood, C. D.; Bradshaw, D.; Rosseinsky, M. J.; Cooper, A. I. *Chem. Commun.* **2006**, 2670–2672.
(20) Tsyurupa, M. P.; Davankov, V. A. *React. Funct. Polym.* **2006**, *66*, 768–779.
(21) Wood, C. D.; Tan, B.; Trewin, A.; Niu, H. J.; Bradshaw, D.; Rosseinsky, M. J.; Khimyak, Y. Z.; Campbell, N. L.; Kirk, R.; Stöckel, E.; Cooper, A. I. *Chem. Mater.* **2007**, *19*, 2034–2048.
(22) Weber, J.; Su, O.; Antonietti, M.; Thomas, A. *Macromol. Rapid Commun.* **2007**, *28*, 1871–1876.
(23) Weber, J.; Antonietti, M.; Thomas, A. *Macromolecules* **2008**, *41*, 2880–2885.
(24) Wood, C. D.; Tan, B.; Trewin, A.; Su, F.; Rosseinsky, M. J.; Bradshaw, D.; Sun, Y.; Zhou, L.; Cooper, A. I. *Adv. Mater.* **2008**, *20*, 1916–1921.
(25) (i) Jiang, J.-X.; Su, F.; Trewin, A.; Wood, C. D.; Campbell, N. L.; Niu, H.; Dickinson, C.; Ganin, A. Y.; Rosseinsky, M. J.; Khimyak, Y. Z.; Cooper, A. I. *Angew. Chem., Int. Ed.* **2007**, *46*, 8574–8578. (ii) Jiang, J.-X.; Su, F.; Trewin, A.; Wood, C. D.; Campbell, N. L.; Niu, H.; Dickinson, C.; Ganin, A. Y.; Rosseinsky, M. J.; Khimyak, Y. Z.; Cooper, A. I. *Angew. Chem., Int. Ed.* **2008**, *47*, 1167–1167.
(26) Jiang, J.-X.; Su, F.; Trewin, A.; Wood, C. D.; Niu, H.; Jones, J. T. A.; Khimyak, Y. Z.; Cooper, A. I. *J. Am. Chem. Soc.* **2008**, *130*, 7710–7720.
(27) Sonogashira, K.; Tohda, Y.; Hagihara, N. *Tetrahedron Lett.* **1975**, 4467–4470.
(28) Jiang, J.-X.; Su, F.; Niu, H. J.; Wood, C. D.; Campbell, N. L.; Khimyak, Y. Z.; Cooper, A. I. *Chem. Commun.* **2008**, 486–488.
(29) Dawson, R.; Su, F.; Niu, H.; Wood, C. D.; Jones, J. T. A.; Khimyak, Y.; Cooper, A. I. *Macromolecules* **2008**, *41*, 1591–1593.
(30) Weber, J.; Thomas, A. *J. Am. Chem. Soc.* **2008**, *130*, 6334–6335.
(31) Rose, M.; Bohlmann, W.; Sabo, M.; Kaskel, S. *Chem. Commun.* **2008**, 2462–2464.
(32) Kobayashi, N.; Kijima, M. *J. Mater. Chem.* **2007**, *17*, 4289–4296.
(33) Kobayashi, N.; Kijima, M. *J. Mater. Chem.* **2008**, *18*, 1037–1045.
(34) Müllen, K.; Scherf, U. *Organic Light-Emitting Devices; 1st* Edition ed.; Wiley-VCH: Weinheim, Germany, 2006.
(35) Skotheim, T. A.; Reynolds, J. R. *Conjugated Polymers - Theory, Synthesis, Properties, and Characterization*, 3rd ed.; CRC Press: Boca Raton, FL, 2007.
(36) Halls, J. J. M.; Walsh, C. A.; Greenham, N. C.; Marseglia, E. A.; Friend, R. H.; Moratti, S. C.; Holmes, A. B. *Nature* **1995**, *376*, 498–500.
(37) Boucle, J.; Ravirajan, P.; Nelson, J. *J. Mater. Chem.* **2007**, *17*, 3141–3153.
(38) Shirota, Y. *J. Mater. Chem.* **2000**, *10*, 1–25.
(39) Shirota, Y. *J. Mater. Chem.* **2005**, *15*, 75–93.
(40) Thelakkat, M. *Macromol. Mater. Eng.* **2002**, *287*, 442–461.
(41) Lee, H. J.; Sohn, J.; Hwang, J.; Park, S. Y. *Chem. Mater.* **2004**, *16*, 456–465.
(42) Wei, P.; Bi, X. D.; Wu, Z.; Xu, Z. *Org. Lett.* **2005**, *7*, 3199–3202.
(43) Roquet, S.; Cravino, A.; Leriche, P.; Aleveque, O.; Frere, P.; Roncali, J. *J. Am. Chem. Soc.* **2006**, *128*, 3459–3466.
(44) Cremer, J.; Bauerle, P. *J. Mater. Chem.* **2006**, *16*, 874–884.
(45) Swager, T. M. *Acc. Chem. Res.* **1998**, *31*, 201–207.
(46) Bennett, A. E.; Rienstra, C. M.; Auger, M.; Lakshmi, K. V.; Griffin, R. G. *J. Phys. Chem.* **1995**, *103*, 6951–6958.
(47) Sun, H. *J. Phys. Chem. B* **1998**, *102*, 7338–7364.
(48) Düren, T.; Millange, F.; Férey, G.; Walton, K. S.; Snurr, R. Q. *J. Phys. Chem. C* **2007**, *111*, 15350–15356.
(49) Sing, K. S. W.; Everett, D. H.; Haul, R. A. W.; Moscou, L.; Pierotti, R. A.; Rouquerol, J.; Siemieniewska, T. *Pure Appl. Chem.* **1985**, *57*, 603–619.
(50) Note that the micropore volume (0.51 cm^3/g) rather than the total pore volume (0.60 cm^3/g) is used to calculate this bulk density value. As such, we are deliberately simulating a microporous domain in the material here and not including any larger pores (small mesopores) which are less easily simulated using this approach.
(51) The $\pi-\pi$ stacked model was also minimized to a target density of 0.83 g/cm^3.
(52) Shen, P.; Sang, G. Y.; Lu, J. J.; Zhao, B.; Wan, M. X.; Zou, Y. P.; Li, Y. F.; Tan, S. T. *Macromolecules* **2008**, *41*, 5716–5722.

(53) Tang, R. P.; Tan, Z. A.; Li, Y. F.; Xi, F. *Chem. Mater.* **2006**, *18*, 1053–1061.
(54) Davankov, V. A.; Pastukhov, A. V.; Tsyurupa, M. P *J. Polym. Sci. B, Polym. Phys.* **2000**, *38*, 1553–1563.
(55) Deng, W. Q.; Xu, X.; Goddard, W. A. *Phys. Rev. Lett.* **2004**, *92*, article no. 166103.
(56) Lee, H.; Choi, W. I.; Ihm, J. *Phys. Rev. Lett.* **2006**, *97*, article no. 056104.
(57) Sabo, M.; Henschel, A.; Froede, H.; Klemm, E.; Kaskel, S. *J. Mater. Chem.* **2007**, *17*, 3827–3832.
(58) Trewin, A.; Darling, G. R.; Cooper, A. I. *New J. Chem.* **2008**, *32*, 17–20.
(59) Cooper, A. I.; Poliakoff, M. *Chem. Commun.* **2007**, 2965–2967.
(60) Ishikawa, M.; Kawai, M.; Ohsawa, Y. *Synth. Met.* **1991**, *40*, 231–238.
(61) Stöckel, E.; Wu, X.; Trewin, A.; Wood, C. D.; Clowes, R.; Campbell, N.:L.; Jones, J. T. A.; Khimyak, Y. Z.; Adams, D. J.; Cooper, A. I. *Chem. Commun.* **2009**, 212–214.

MA802625D